

Dissociative and non-dissociative adsorption dynamics of N₂ at Fe(110)

I.Goikoetxea,^{1,2,*} M. Alducin,^{1,2,†} R. Díez Muiño,^{1,2,‡} and J.I. Juaristi^{3,1,2,§}

¹*Centro de Física de Materiales (CSIC-UPV/EHU) - Materials Physics Center MPC,*

P. Manuel de Lardizabal 5, 20018 San Sebastián, Spain

²*Donostia International Physics Center DIPC,*

P. Manuel de Lardizabal 4, 20018 San Sebastián, Spain

³*Departamento de Física de Materiales, Facultad de Químicas,*

Apartado 1072, 20080 San Sebastián, Spain

Abstract

We study the adsorption dynamics of N₂ on the Fe(110) surface. Classical molecular dynamics calculations are performed on top of a six-dimensional potential energy surface calculated within density functional theory. Our results show that N₂ dissociation on this surface is a highly activated process that takes place along a very narrow reaction path with an energy barrier of around 1.1 eV, what explains the measured low reactivity of this system. By incorporating energy exchange with the lattice in the dynamics, we also study the non-dissociative molecular adsorption process. From the analysis of the potential energy surface, we observe the presence of two distinct N₂ adsorption wells. Our dynamics calculations show that the relative population of these adsorption sites varies with the incident energy of the molecule and the surface temperature. We find an activation energy of around 150 meV that prevents molecular adsorption under thermal and hypothermal N₂ gas exposure of the surface. This finding is also consistent with the available experimental information.

PACS numbers: 34.35.+a, 79.20.Ap, 79.20.Rf

* itziar.goicoechea@ehu.es

† wapalocm@ehu.es

‡ rdm@ehu.es

§ josebainaki.juaristi@ehu.es

I. INTRODUCTION

Understanding the interaction of N_2 with Fe has an undeniable interest in surface chemistry. The reason is that Fe is the traditional catalyst for ammonia synthesis, for which N_2 dissociation is the rate-limiting step [1, 2]. This has motivated an extensive research over the years, from both the theoretical and experimental side, directed to extract the properties controlling such a fundamental process and, even more generally, the N_2 -Fe interaction.

As observed on the W surfaces [3, 4], the rate of nitrogen adsorption on Fe is face specific. Among the low crystallographic index surfaces, Fe(111) and Fe(110) constitute the extreme examples of the most and less reactive faces [5, 6]. Early investigations aimed to characterize the interaction of N_2 with Fe(111) identified two distinct molecular species on this face [7–10]: a weakly bound state with the molecular axis normal to the surface and a more strongly bound state with the molecule lying parallel to the surface. Using photoelectron spectroscopy and high-resolution electron energy loss spectroscopy, the latter was identified as the immediate precursor state to dissociation [7]. Molecular beam experiments directed to probe the dynamics of the $\text{N}_2/\text{Fe}(111)$ system showed that the N_2 translational kinetic energy can be efficiently used to promote reactivity on this surface [11]. The initial dissociative adsorption probability increases by a factor of 10^5 , rising from 10^{-6} at 0.09 eV to 10^{-1} at 4.3 eV, approximately. Whether dissociation is a direct process at high N_2 energies or mediated by a molecular adsorption state, as in low-pressure exposure experiments, could not be conclusively resolved.

Interaction of N_2 with the less reactive Fe(110) has also attracted great interest [12–17]. However, there are certain discrepancies among the different studies that have not been solved yet. Calculations performed with density functional theory (DFT) predict activation energies for N_2 dissociation at this surface in the range of 1.1-1.2 eV [15, 16]. These values are much larger than the value of 0.28 eV obtained experimentally [6]. The discrepancy led the authors to suggest that the measured dissociation of N_2 on Fe(110) was a process dominated by atomic steps and defects [15]. More recently, studies on the energetics of N_2 on this surface have been presented in the context of the synthesis of boron nitride nanotubes [17]. An interesting result of the theoretical works of refs. 16 and 17 is the different adsorption geometry they obtain for the N_2 molecule on Fe(110). Whereas in ref. 16 the adsorption position is identified for the N_2 molecule located with its axis perpendicular to

the surface over the top site, in ref. 17 the most stable adsorption configuration corresponds to the molecule lying parallel to the surface with its center of mass on the hollow site. Interestingly, the results of ref. 17 would be in accordance with the adsorption species identified experimentally on the Fe(111) surface. However, there are no experimental information on the Fe(110) face to clarify this point.

Motivated by all these previous studies and the remaining uncertainties that this simple system still raises, we have performed a theoretical study of the $\text{N}_2/\text{Fe}(110)$ dynamics. Our objective is to understand the low reactivity of this system and fully characterize the interaction of N_2 with the Fe(110) surface and its adsorption properties. With this aim, we start in Section II by performing a static analysis of the molecule-surface interaction, based on the *ab-initio* six-dimensional (6D) potential energy surface (PES). The latter is calculated for the different positions of the two N atoms in the molecule within the frozen surface approximation, i.e., keeping the positions of the Fe atoms fixed. This analysis allows us to identify the possible atomic and molecular adsorption states, explore the existence of reaction paths to dissociation and make a first estimate of the possible activation energies for different reaction processes. In the following two sections we study the adsorption dynamics of N_2 on Fe(110). We start by analyzing the dissociative adsorption in Section III. To study this process, we perform adiabatic classical dynamics calculations on the precalculated 6D PES for different initial energies and incident angles of the N_2 molecule. Since in its interaction with the surface the molecule moves in a multidimensional configuration space, only this kind of simulations can be conclusive in terms of identifying the actual reaction paths followed by the dissociating molecules, and answer questions such as if dissociation occurs directly or, on the contrary, it is governed by a precursor state. Additionally, dissociative adsorption probabilities as a function of the molecule initial translational energy and incidence angle are presented. The results for molecular adsorption are shown and discussed in Section IV. During such process, the molecule loses energy up to be thermalized with the surface on one of the possible adsorption wells. Therefore, we have to go beyond the adiabatic and frozen surface approximations in order to describe them. In this work, energy exchange and dissipation between the molecule and the surface are included in the classical dynamics simulations by applying the generalized Langevin oscillator model (GLO) [18]. The influence of surface temperature and the incidence energy is also analyzed. The main conclusions of the paper are summarized in Section V.

II. CALCULATION OF THE ADIABATIC POTENTIAL ENERGY SURFACE

In an adiabatic picture, the interaction of N_2 with the $\text{Fe}(110)$ surface is described within the frozen surface approximation by a 6D PES that depends on the position of the molecule. The latter can be defined in terms of the center of nuclear mass, $\mathbf{R}=(X,Y,Z)$, the molecular interatomic distance r and the molecular orientation relative to the surface determined by the polar and azimuthal angles (θ, φ) . The coordinate system used in the present study is depicted in Fig. 1.

The adiabatic 6D PES for $\text{N}_2/\text{Fe}(110)$ is constructed from the interpolation of 20130 *ab initio* energies that are calculated with spin-polarized DFT to assure an adequate description of the magnetic nature of Fe. Interpolation is performed with the *corrugation reducing procedure* (CRP) [19] that requires the calculation of the three dimensional (3D) $\text{N}/\text{Fe}(110)$ PES also. Briefly, the CRP consists in reducing the corrugation of the $\text{N}_2/\text{Fe}(110)$ PES by subtracting from it the potential energy between each of the N atoms forming the molecule and the $\text{Fe}(110)$ surface (the $\text{N}/\text{Fe}(110)$ is used at this stage). The resulting 6D energy surface, denoted as “the 6D interpolation function” in ref. 19, exhibits a smoother dependence on the coordinates (X,Y,θ,ϕ) and permits us to interpolate it within the required accuracy for treating low energy gas/surface dynamics.

All DFT data have been obtained using the “Vienna *ab initio* simulation program” [20, 21] (VASP) that operates with a plane-wave basis set. We performed a series of preliminary calculations to determine the computational settings that provide an efficient and accurate calculation of the $\text{N}_2/\text{Fe}(110)$ PES. The exchange correlation (XC) energy is calculated within the generalized gradient approximation (GGA) and the Revised Perdew-Burke-Ernzerhof energy functional (RPBE)[22]. The electron-core interaction is treated in the plane augmented wave (PAW) approximation [23]. The energy cut-off in the plane-wave expansion is 400 eV. The fractional occupancies are determined through the broadening approach of Methfessel and Paxton with $N=1$ and $\sigma=0.4$ eV [24]. The energy criteria for total energy self-consistency is 10^{-5} eV.

The theoretical lattice constant obtained using these computational settings and a $15 \times 15 \times 15$ Monkhorst-Pack k -point mesh is $a=2.86$ Å. The corresponding bulk interlayer spacing of $d=2.05$ Å for the (110) direction is in good agreement with the nominal value of $d=2.03$ Å. The $\text{Fe}(110)$ surface is next modeled by a periodic five-layer slab with a (2×2) surface unit

cell and a supercell vector along the normal to the surface (Z -axis) of $15d$, from which $10d$ corresponds to vacuum. This supercell size allows an efficient calculation of the DFT energy grid used in the interpolation, while assuring a significant reduction of undesirable interactions among the periodically repeated molecules, as discussed below. The Brillouin-zone integration in this large supercell is performed with a $4 \times 4 \times 1$ Monkhorst-Pack grid of special k -points. As a first step, the clean Fe(110) slab is relaxed to get the equilibrium geometry of the surface. Keeping the third layer fixed, no shift in any of the directions is obtained, in agreement with preceding theoretical results [14]. Our computational settings to represent the Fe(110) surface also give a reasonable description of the magnetic properties, being $2.68\mu_B$ the surface magnetic moment per Fe atom of the topmost layer.

Using the same supercell, we proceed by calculating the energy $E(r)$ of the isolated N_2 as a function of the distance r between the two N atoms. This allows us to obtain the value $r_{eq}=1.11 \text{ \AA}$ for the N-N equilibrium distance and $E_{diss}(N_2)=-9.891 \text{ eV}$ for the dissociation energy of the molecule. The latter is calculated as $E_{diss}(N_2) = 2E(N) - E(N_2) + E_{ZPE}$, where $E(N)$ is the energy of the isolated N atom, $E(N_2)$ the energy of the isolated N_2 calculated at the equilibrium distance r_{eq} , and E_{ZPE} is the zero point energy of 0.147 eV , which is obtained by solving the 1D Schrödinger equation for $E(r)$. These results compare well with the experimental bond length and binding energy of 1.0975 \AA and 9.803 eV , measured for N_2 in gas phase [25]. The $E(r)$ curve is also calculated including the Fe(110) slab and locating the N_2 molecule in the middle of the vacuum space. The r_{eq} and E_{diss} values differs in less than 1% from those obtained in the isolated- N_2 calculation, confirming the adequacy of the supercell size to calculate the $N_2/\text{Fe}(110)$ PES.

Next, the calculation of the N/Fe(110) three-dimensional 3D PES and the $N_2/\text{Fe}(110)$ 6D PES are performed keeping the geometry of the slab along the three axis fixed (frozen surface approximation). The use of this approximation in gas/surface dynamics simulations is justified as long as the processes we are interested in take place in a time interval short enough not to be influenced by surface relaxation.

A. N/Fe(110) PES

To build the N/Fe(110) 3D PES, energies are calculated for 13 different positions of the N atom over the surface unit cell. By symmetry, they provide information on the 15 sites

depicted in Fig. 1(b) by black and white circles. For each site, the distance Z_N of the N atom is varied from -1.2 \AA below the surface to 6 \AA above the surface in steps of 0.1 \AA . The surface is defined by the topmost Fe layer. At $Z_N=6 \text{ \AA}$ all the energy curves have steadily merged to the same asymptotic value that is taken as the zero reference energy in the following [26]. The 3D N/Fe(110) PES is constructed by interpolating the spin-polarized DFT data with the 3D CRP [19]. At this point, we follow the same procedure and numerical methods used in ref. 27 for the N/W(110) PES.

The minimum energy configuration corresponds to the N atom on the threefold site at $Z_N \sim 1.0 \text{ \AA}$ from the topmost atomic layer. The adsorption energy for atomic nitrogen at this site is $E_{ads}(N) = -5.75 \text{ eV}$, which is just marginally larger than the value we obtain at the hollow site (-5.72 eV). Considering the calculated N_2 dissociation energy in vacuum (-9.891 eV) and defining the dissociative adsorption energy per molecule as, $E_{diss-ads}(N_2) = 2E_{ads}(N) - E_{diss}(N_2)$, we obtain that the N_2 dissociative adsorption is an exothermic process on the Fe(110) surface that liberates 1.61 eV . This value compares quite well with the value of -1.45 eV reported by Mortensen *et al.* [14] using the revPBE XC-functional. In that reference, relaxation of the first two Fe layers in the direction normal to the surface was allowed. Under these conditions, it was found that the threefold site is the equilibrium position of the adsorbed N atom in agreement with our frozen surface calculations. Using the PW91 XC-functional, Pick *et al.* [28] reported a dissociative adsorption energy of -2.56 eV , and noticed that a lower value of 0.79 eV (in absolute value) is obtained per N_2 molecule when using the RPBE functional. This implies $E_{diss-ads}(N_2) = -1.77 \text{ eV}$, i.e., a value slightly more exothermic than the one we find here with the same functional. We attribute the difference to the fact that Pick *et al.* allow full relaxation of the upper three Fe layers and of the N atom. In doing so, the authors find that the N atom preferably adsorbs on the hollow site, for which we obtain a marginally higher energy instead. The reason is that, when full relaxation is allowed, the four Fe atoms surrounding the N atom change their arrangement from rhombus to almost square structure, producing a quasi fourfold adsorption site [28]. The same surface reconstruction is reported by Riikonen *et al.* [17], who also allowed full relaxation of the top most layers. Using the PBE XC-functional, that is known to typically provide larger adsorption energies than the RPBE, these authors obtain adsorption energies of -6.6 eV and -6.3 eV for N on the quasi fourfold hollow site and on the threefold site, respectively. Clearly, surface relaxation is a necessary requirement to provide an accurate

description of N adsorption on the Fe(110) surface. However, it is worth to note that we neglect it here because the surface reconstruction is in our case irrelevant and even counterproductive for our only purpose of using the N/Fe(110) PES to reduce the corrugation in the 6D N₂/Fe(110) PES.

The dependence of the N/Fe(110) PES on the distance of the N atom from the surface is shown in Fig. 2. In panel (a), this dependence is plotted for selected positions over the surface unit cell that are used in the interpolation procedure. Note the small energy differences obtained for the threefold site (denoted long th-hollow in the figure) and the hollow site. The accuracy of the constructed 3D PES is checked by comparing a set of DFT energies not used in the interpolation with their corresponding CRP interpolated values. In Fig. 2(b), we show three representative examples of the interpolation quality for any position (X_N, Y_N, Z_N) of the N atom.

B. N₂/Fe(110) PES

DFT data are calculated for 30 different configurations of the N₂ molecule. A configuration is defined by the molecular orientation (θ, φ) and the position of the molecular center over the surface unit cell (X, Y) . For each configuration, a 2D (r, Z) -cut of the PES is obtained with r varying from 0.71 Å to 2.31 Å in a non-equidistant grid of 11 points, and Z from 0.0 to 6.0 Å by steps of 0.1 Å. We observe that for each r value, the energy of all the configurations for a given r -value is basically constant for $Z \geq 6$ Å. Thus, the zero reference energy in the N₂/Fe(110) PES is taken for the molecule with the bond length r_{eq} and located at 6 Å from the surface. The potential energies are calculated for the following configurations [black circles in Fig. 1(b)]:

- Six configurations over top site ($X=0, Y=0$): $\theta=0^\circ$; $\theta=90^\circ$ with $\varphi=0^\circ$ and $\varphi=54.74^\circ$; and $\theta=45^\circ$ with $\varphi=0^\circ$, $\varphi=54.74^\circ$ and $\varphi=90^\circ$.
- Five configurations over hollow (hw) site ($X=a/2, Y=0$): $\theta=0^\circ$; $\theta=90^\circ$ with $\varphi=0^\circ$ and $\varphi=90^\circ$; and $\theta=45^\circ$ with $\varphi=0^\circ$ and $\varphi=90^\circ$.
- Six configurations over bridge (br) site ($X=a/4, Y=a\sqrt{2}/4$): $\theta=0^\circ$; $\theta=90^\circ$ with $\varphi=0^\circ$, $\varphi=54.74^\circ$, and $\varphi=125.26^\circ$; and $\theta=45^\circ$ with $\varphi=54.74^\circ$ and $\varphi=125.26^\circ$.

- Six configurations over short top-hollow (short th) site ($X=a/4, Y=0$): $\theta=0^\circ$; $\theta=90^\circ$ with $\varphi=0^\circ$ and $\varphi=54.74^\circ$; and $\theta=45^\circ$ with $\varphi=0^\circ$, $\varphi=90^\circ$, and $\varphi=180^\circ$.
- Seven configurations over long top-hollow (long th) site ($X=a/4, Y=a\sqrt{2}/4$): $\theta=0^\circ$; $\theta=90^\circ$ with $\varphi=90^\circ$ and $\varphi=35.26^\circ$; and $\theta=45^\circ$ with $\varphi=0^\circ$, $\varphi=54.74^\circ$, $\varphi=90^\circ$, and $\varphi=270^\circ$.

These *ab initio* data are interpolated with the 6D CRP [19]. Briefly, interpolation is performed on the less corrugated function I^{6D} . The latter is calculated for each *ab initio* potential energy V^{6D} as,

$$V^{6D}(X, Y, Z, r, \theta, \varphi) = I^{6D}(X, Y, Z, r, \theta, \varphi) + V^{3D}(X_A, Y_A, Z_A) + V^{3D}(X_B, Y_B, Z_B), \quad (1)$$

where V^{3D} is the N/Fe(110) potential energy and $(X_{A,B}, Y_{A,B}, Z_{A,B})$ are the coordinates of the two N nuclei in the molecule. Following ref. 27, I^{6D} is interpolated with a third order spline interpolation over the molecular center of (nuclear) mass coordinates (X, Y, Z) and over the internuclear distance r . Interpolation over θ and φ is done with a Fourier series expansion.

Some representative interpolated energy curves as a function of Z , together with the DFT data from which they are obtained, are shown in Fig. 3(a) for different configurations of the molecule. The accuracy of the constructed 6D PES is checked by comparing the interpolated values with calculated DFT data not included in the interpolation procedure. In Fig. 3(b) we show this kind of comparison for a given set of configurations as good examples of the high accuracy obtained in the interpolation. We have observed that the main source of errors is caused by the difficulty to interpolate over θ and φ . However, as the representative examples in Fig. 4 show, this problem has been reasonably controlled by our choice of configurations, which includes various molecular orientations at each position over the surface unit cell.

In short, interpolation errors are small on average (≤ 50 meV) for distances above 2.5 Å from the surface. Below this distance, errors are kept below 100 meV for those configurations that are relevant in the dynamics. In the highly repulsive regions of the PES, interpolation errors can be larger, but these regions are neither probed by the reflected molecules nor by the dissociated ones.

C. Properties of the adiabatic 6D N₂/Fe(110) PES

A selection of (r, Z) cuts of the N₂/Fe(110) PES is shown in Fig. 5. One remarkable feature is the presence of possible molecular adsorption sites [Figs. 5(a) and (b)]. These two configurations have been carefully analyzed in order to confirm that the apparent minima in the (r, Z) cuts correspond to local minima in the 6D PES. Such analysis is carried out through the classical trajectory code as proposed in ref. 29. This method also allows to measure the diffusion and desorption barriers from the local minimum. Briefly, the procedure consists in performing a series of 6D trajectory calculations that start with the molecule at the 6D position where a local minimum is expected. Starting with zero kinetic energy E_i , the confinement of the trajectories in the well is probed for increasing E_i using a Monte-Carlo sampling of all possible initial velocity orientations associated with E_i . The diffusion (desorption) barrier height corresponds to the threshold value of E_i for which diffusion (desorption) out of the well is obtained. Zero-point energy corrections are not considered in this analysis. With this procedure, we confirm the configurations of Figs. 5(a) and (b) as two local minima for possible molecular adsorption. For the deepest minimum, a molecular adsorption energy of roughly -298 meV is found. In this adsorption well, the molecule lies parallel to the surface ($\theta = 90^\circ$, $\varphi = 90^\circ$), with its center of mass over the hollow site at $Z \sim 1.4$ Å and with an interatomic distance $r \sim 1.21$ Å [Fig. 5(a)]. The latter means that potentially adsorbed molecules are stretched around 10% from the internuclear equilibrium distance in vacuum ($r_{eq} = 1.11$ Å). The energy barrier measured from the bottom of this well that allows the molecule to escape towards desorption is ~ 480 meV. The less deep potential well of roughly -184 meV corresponds to the molecule perpendicular over the top site at $Z \sim 2.4$ Å and $r \sim r_{eq}$ [Fig. 5(b)]. From the bottom of this well, the minimum energies to escape towards desorption and towards the deepest adsorption well are 320 meV and 330 meV, respectively.

The ontop adsorption configuration is the only one reported by Logadottir *et al.* [16]. Using the RPBE XC-functional the authors found an adsorption energy of about -0.27 eV. More recently, Riikonen *et al.* [17] reported the existence of the two molecular adsorption configurations we find, but with significantly larger adsorption energies (-1.1 eV and -0.5 eV for N₂ on the hollow and top sites, respectively). We have verified that when surface relaxation is allowed as in ref. [17], the depths of our adsorption wells increase in about

100 meV. Thus, the still existing differences with our results can be attributed to the use of the PBE XC-functional, which is known to give larger adsorption energies than the RPBE one used here. Interestingly, we will show in Section IV that even if N_2 adsorption over the hollow site is energetically the most favorable state, the less deep well plays an important role in the adsorption characteristics of N_2 on Fe(110) at low surface temperatures and low incidence energies of the molecule.

The 2D cut of Fig. 5(c) corresponds to the configuration with the *ab initio* minimum barrier to dissociation. From the 30 configurations for which *ab initio* data have been calculated, this is the only one that might lead to dissociation at low energies. In this case, the molecule is located on a bridge site with the molecular axis parallel to the surface ($\theta = 90^\circ$) and pointing towards hollow sites ($\varphi = 125.26^\circ$). Within this configuration, the contourplot shows that the activation energy for dissociation is approximately 1.1 eV. Hence, a simple and static analysis of these (r, Z) cuts, where the molecule is forced to approach the surface with a fixed configuration, leads to the conclusion that the dissociative adsorption in the $\text{N}_2/\text{Fe}(110)$ system is activated. Nevertheless, since the molecular initial configuration can be continuously altered along the trajectory due to its interaction with the surface, a conclusion based only on the analysis of the PES for the different but fixed configurations can be misleading [3, 30].

III. DISSOCIATIVE ADSORPTION OF N_2 MOLECULES ON THE FE(110) SURFACE

In this section we analyze the reaction dynamics of N_2 on the Fe(110) surface. With this aim, we perform classical trajectory calculations on the precalculated adiabatic PES. Trajectories start with the N_2 molecule at its equilibrium bond length r_{eq} and at $Z=6$ Å. The zero point energy of the molecules is neglected. Under these initial conditions, the PES value is zero as discussed in Section II B. For each incidence energy E_i and angle of incidence Θ , a conventional Monte Carlo procedure is used to sample the initial positions (X, Y) over the unit cell, the azimuthal incidence angle of the molecular beam, and the molecular orientation (θ, φ) . In the trajectory calculations, the following events are distinguished: (i) dissociation, if the molecule has a positive radial velocity and the internuclear distance is larger than $2r_{eq}$ (in particular, $r \geq 2.225$ Å); (ii) reflection, if the molecular center of mass reaches the starting

point $Z=6$ Å with a positive Z velocity; and (iii) molecular trapping, when the molecule is neither dissociated nor reflected after 15 ps. For the incidence conditions studied in this section all trajectories are either dissociated or reflected well before reaching the integration time of 15 ps. The typical dissociation and reflections times are below one ps. Furthermore, no molecular trapping events are observed.

Results for the initial dissociative sticking probability S_0 plotted versus both the initial incident energy E_i and the normal incident energy $E_i \cos^2 \Theta$ are shown in Fig. 6, for different incidence angles Θ . The sticking probability for each (E_i, Θ) is obtained from the evaluation of a minimum of 50000 trajectories. This unusual large number is necessary to ensure sufficiently good statistics, given the low reactivity of this system.

The dissociation probability curves show the characteristic behavior of an activated system. Let us focus first in the results obtained under normal incidence conditions ($\Theta=0^\circ$). For initial energies below 1.6 eV, there are no sticking events out of the 50000 calculated trajectories. This means that the dissociation probability of N_2 in Fe(110) below this energy is lower than 2×10^{-5} . Note that the dynamics simulations provide an energy threshold for dissociation much larger than the energy barrier of 1.1 eV observed from the direct inspection of the PES [Fig. 5(c)]. This result, i.e., the extremely low reaction probabilities obtained up to energies substantially higher than the barrier of 1.1 eV, evidence a reaction path characterized by a reduced configurational space.

A schematic idea of the dynamics leading to dissociation can be obtained with help of Figs. 7 and 8. The results are shown for normal incidence and two incidence energies, $E_i=3$ and 4 eV. We note that the dynamics at $E_i=3$ eV is still representative of what happens close to the activation energy and it has the advantage of providing an adequate statistical description of the dissociation dynamics in the lower energy range. In both figures upper plots represent the position of the center of mass of the molecule over the surface unit cell, when the molecule first reaches the distance Z from the surface. At each Z , the percentage of dissociating molecules N_z is written on top of each panel together with the total percentage of molecules reaching Z respectively. The rotational motion of the dissociating molecules is represented in the lower plots that show the corresponding polar distribution as they approach the surface.

Focusing in the dissociating molecules, we have verified that the (X, Y) positions and θ distribution of the molecules at $Z=2$ Å are roughly the ones at the initial point of the trajec-

tories. The reduction of N_z below $Z=1.4 \text{ \AA}$ shows that molecules start to dissociate below this Z value. An important observation is that dissociation is a direct process occurring without the participation of any precursor state. More precisely, following the evolution of the dissociating molecules, it is apparent in both figures that the previously identified molecular adsorption wells at top and hollow sites play no role in the dissociation dynamics. Note also that most of the dissociating molecules have an initial orientation parallel to the surface. The narrowing of the angular distributions below 2 \AA shows that this is indeed the preferential orientation to reach dissociation. Apart from this slight θ rotation, we observe no substantial motion of the molecules along the surface plane. In the high energy case ($E_i=4 \text{ eV}$), for which the molecules can overcome a large amount of energy barriers, dissociation occurs along the diagonals joining the top-bridge sites. Even in this case, more than two thirds of the molecules dissociate in regions close to the bridge site, instead of dissociating in regions close to the top site. This behavior is accentuated at the lower incidence energy, $E_i=3 \text{ eV}$. In the latter case, the dissociating molecules are concentrated close to the bridge sites, even though the incidence energy is around 2 eV higher than the minimum energy barrier for dissociation found at this position. This observation proves the narrowness of the reaction path, i.e., that the number of configurations with energy barriers for dissociation close to the minimum value of about 1.1 eV constitutes a very small fraction of the total 6D configuration space.

The dependence of the dissociation probability on the incidence angle Θ is intriguing. The first feature apparent from Fig. 6 is that neither total energy scaling nor normal energy scaling is observed. On the one hand, the dissociation probability is larger the higher is the normal energy for equal total energy [Fig. 6(a)]. On the other hand, the dissociation probability increases with total energy for equal normal energy, except for incidence angles larger than 45° for which normal energy scaling is observed [Fig. 6(b)]. The analysis of our 6D molecular dynamics calculations shows that the reason for this behavior is that, for energies close to the normal energy threshold, the dissociating molecules have to overcome energy barriers of around $0.5\text{-}0.6 \text{ eV}$ at distances $Z \simeq 2.0 - 2.5 \text{ \AA}$. For illustrative purposes, we analyze in more detail the energetics of the configuration with the minimum dissociation barrier shown in Fig. 5(c). In Fig. 9 we show the potential energy as a function of the reaction coordinate s . The latter is defined as the distance in the (Z, r) space measured from the position of the minimum energy barrier to dissociation along the minimum energy

path [depicted by a red line in the contour plot of Fig. 5(c)]. Interestingly, Fig. 9 shows that apart from the above mentioned late barrier of around 1.1 eV, a second lower barrier of around 0.6 eV appears in the entrance channel. At the position of this lower barrier, the interatomic distance is roughly r_{eq} and $Z=2$ Å. The actual 6D reaction paths followed by the dissociating molecules depend on the energy and angle of incidence, and generally do not coincide with the represented 2D path. However, as explained above, we have checked that for low energy reacting molecules, all these reaction paths present energy barriers in the entrance channel similar to the one shown in Fig. 9. The presence of these barriers in the entrance channel, where the dissociative dynamics is still controlled by the normal energy, explains the results shown in Fig. 6. Even if the molecule may have enough total energy to overcome the dominant late barriers, for off-normal incidence conditions the normal energy may be insufficient to overcome the lower barriers at the entrance channel. As a result, the sticking probability in Fig. 6(a) decreases while increasing the incidence angle for the same total energy. In the same way, once the normal energy is enough to overcome the barriers in the entrance channel, the probability to surmount the late barriers for equal normal energy must increase with total energy. This explains the behavior observed in Fig. 6(b) showing that for equal normal energy, the sticking probability increases with incidence angle, i.e., with total energy. The normal energy scaling is obtained for $\Theta > 45^\circ$ because at such large angles the total energy associated with the minimum normal energy of ~ 0.6 eV is already larger than the late barrier of 1.1 eV.

Let us finish this section by discussing our results in the light of what is known about this system. First, the low reactivity of the Fe(110) surface for N_2 uptake [5, 6] is consistent with the negligible values of the sticking probability obtained for incidence energies below 1.6 eV. We find that this result is due to the presence of high energy barriers for dissociation, together with the small fraction of the 6D configuration space that corresponds to molecular configurations with energy barriers close to the minimum. Our full 6D dynamics calculation confirms the dissociation barriers calculated in refs. 15 and 16. The agreement is remarkable given that in these previous works the analysis of the dissociation process is not performed on the 6D PES, but on a restricted region of the configurational space. This kind of low dimensional studies usually implies a series of assumptions to identify the starting initial state and the minimum energy reaction path. Our 6D results show that the transition state and the corresponding activation energies are well identified in both references, despite

dissociation does not proceed through any of the N_2 adsorption states as assumed there. What our full 6D dynamics simulations additionally show is that the configuration space leading to dissociation is so restricted that, in practice, the dissociation probabilities will remain below 10^{-5} up to energies well above the minimum activation energy of about 1.1 eV. In this respect, our calculations also support the conclusion of ref. 15 according to which the lower dissociation barriers measured in ref. 5 are probably due to dissociation at steps.

IV. ENERGY EXCHANGE WITH THE SURFACE AND MOLECULAR ADSORPTION

Motivated by the existence of the two N_2 adsorption wells, we have also studied the molecular adsorption of N_2 on Fe(110). Within the adiabatic and the frozen surface approximations used in the previous section, energy exchange and dissipation between the molecule and the surface are neglected. Since within this framework the total energy of the molecule along the trajectory is conserved, molecular adsorption processes requiring that the molecule loses energy in order to be accommodated in the adsorption well, cannot be modeled. For this reason, we have performed a new set of classical dynamics calculations that include energy exchange and dissipation between the molecule and the lattice in the equations of motion.

Using the adiabatic $\text{N}_2/\text{Fe}(110)$ PES, we describe the N_2 -surface coupling through the generalized Langevin oscillator (GLO) model [18], as implemented in ref. 31. This model represents the surface motion in terms of a 3D harmonic oscillator with mass equal to the Fe atomic mass. Dissipation and thermal fluctuations are included through the second fluctuation-dissipation theorem with the help of a second 3D oscillator of identical mass, known as the *ghost* oscillator, that is subject to a friction and to a random force. The *ghost* oscillator represents the “thermal bath” that the bulk provides. The frequencies associated to the surface and the ghost oscillators are represented by the surface phonon frequencies close to the edges of the Fe(110) surface Brillouin zone, namely, $\omega_x = \omega_y = 1.2 \times 10^{-3}$ a.u. (atomic units) and $\omega_z = 6.6 \times 10^{-4}$ a.u. [32]. The value used for the friction coefficients associated to the *ghost* oscillator is 7×10^{-4} a.u. [18]. We have checked that our result are not very sensitive to the exact value of these parameters, as long as we keep the same order of magnitude. The results shown in this section for each incidence condition and surface

temperature have been obtained from the analysis of 5000 trajectories. This number turns to be enough for the statistical analysis of the molecular adsorption process.

In the following, a molecular adsorption event is identified whenever the molecule that is neither reflected nor dissociated after 15 ps fulfills the following final conditions: (i) its total energy (kinetic plus potential) is negative, i.e., lower than the potential energy of the molecule at r_{eq} and $Z=6$ Å and (ii) the total energy of the system (molecule and surface) is also negative. On the one hand, the first energy restriction guarantees that the molecule will not be able to escape to vacuum and that it is already well accommodated in one of the molecular adsorption wells. On the other hand, the second restriction is a strict condition assuring that there is not enough energy left in the system that could eventually be adsorbed by the molecule to escape into vacuum. The dissociation and reflection events are defined as in previous section. For surface temperatures below 300 K and the incidence energies E_i used here, all molecules are either dissociated, reflected, or molecularly adsorbed after the integration time of 15 ps. For the simulations at $T_s=500$ K, there is a non-negligible percentage of molecular trapping, i.e., molecules that after the integration time of 15 ps are not dissociated, reflected, or molecularly adsorbed. However, we have verified that increasing the integration time to 30 ps the number of molecularly adsorbed events, defined by the conditions (i) and (ii), is practically the same. Thus, the results for molecular adsorption are rather robust, since an increase in the integration time will imply even smaller total energies for the adsorbed molecules, closing any possibility for reflection. Furthermore, dissociation from the molecular adsorption well is also unlikely in view of the large minimum energy barrier found for this process.

The results of our calculations for molecular adsorption under normal incidence conditions are shown in Fig. 10. The adsorption probability for molecules is plotted as a function of E_i for T_s varying in the range 80-500 K. For the incidence energies and surface temperatures considered here, the adsorption probability tends to decrease when increasing T_s . Note that in all cases $E_i > k_B T_s$, that is, molecules are *hot* compared to the surface and, as a result, energy is transferred in average from the former to the latter. As T_s increases, the surface-molecule energy difference becomes smaller and less energy is dissipated from the molecule to the lattice. Thus, the possibility of trapping on any of the adsorption wells is reduced. Focusing on the E_i -dependence, we observe that the curves exhibit a similar shape for the calculated T_s . In all cases, there is a minimum incidence energy of around

0.15 eV to obtain molecular adsorption. Furthermore, the adsorption probabilities increase monotonously with E_i up to reaching a maximum at ~ 0.75 eV. At the lowest temperatures, the maximum adsorption probability is about 60%, a rather high value if we compare it with the dissociation probabilities obtained in this system, for instance. The appearance of a threshold energy and the increase of the adsorption probability at low energies is due to the presence of energy barriers in the entrance channel that the molecules have to overcome to arrive to the adsorption wells. Above 0.75 eV, the adsorption probability decreases because the energy exchange with the lattice is insufficient for the molecules to lose all the energy required to accommodate in the adsorption wells. Note that the reported energy barrier of 0.15 eV prevents molecular adsorption under thermal and hypothermal N_2 gas exposure of the surface, in agreement with experiments [13].

Next, we analyze how the molecules are distributed among the two possible adsorption wells we have identified in this system: the hollow-parallel state and the top-vertical state [Figs. 5(a) and (b), respectively]. The molecular adsorption probability in each of the adsorption wells are represented as a function of E_i in Fig. 11. The fraction of molecules adsorbed in each well is shown in the inset. Though, as explained above, the most stable adsorption state is the one with the molecule over the hollow site, Fig. 11 shows that below 250 meV this well is not populated and the molecules adsorb on the top-vertical well instead. For instance, at 80 K, this well remains as the preferential adsorption state up to incidence energies of ~ 650 meV. Above this energy, a larger amount of molecules adsorb on the most stable hollow-parallel well. At $E_i=3$ eV, almost all molecules end on this state. Though this general behavior is observed for all the surface temperatures, as T_s increases the relative weight of the top-vertical state in the adsorption probability decreases. All these observations can be explained as follows.

The different energy dependence of the adsorption probability in the two sites is related to the different energy barriers that the molecules have to overcome before being adsorbed on one or the other state. More precisely, the minimum barrier for adsorption on the top-vertical state is 150 meV, whereas it is around 250 meV for the hollow-parallel adsorption. When using the less repulsive PW91 exchange-correlation functional [33] the values of the calculated barriers are 14 meV and 100 meV, respectively, but the adsorption process remains activated. As E_i and T_s increase, energy dissipation from the molecule to the surface becomes less efficient. Hence, the probability to be adsorbed on the top-vertical well of

-184 meV decreases more rapidly than the adsorption probability on the most stable and deeper adsorption well of -298 meV. We want to emphasize that, these results of the dynamics show that even if a static analysis would lead us to think that all molecules are trapped in the deeper well, i.e., the hollow-parallel well, only by performing classical dynamics calculations the real trend can be known. For this reason, it is not enough to identify the most stable site in a total energy calculation to gain knowledge on the adsorption properties of this system. As we show, the final adsorption site can depend on the surface temperature and on the kinetic energy of the impinging molecules.

According to our simulations, N_2 adsorption on $\text{Fe}(110)$ exhibits some similar features to what has been observed on the $\text{Fe}(111)$. The top-vertical and hollow-parallel states could be associated to the $\gamma\text{-N}_2$ and $\alpha\text{-N}_2$ observed on the $\text{Fe}(111)$ surface. Also in that surface the weakly bound state $\gamma\text{-N}_2$ corresponds to the molecule with the axis perpendicular to the surface, while the $\alpha\text{-N}_2$ one is lying parallel. As T_s increases, we obtain on the $\text{Fe}(110)$ surface that the adsorption probability decreases more rapidly on the top-vertical than on the hollow-parallel N_2 . Furthermore, the former state dominates the adsorption process for incidence energies below 0.75 eV, while the latter does above that energy. These observations, which are related with the lower adsorption energy of the top-vertical state as compared with that of the hollow-parallel, seem compatible with the different desorption temperatures of the $\gamma\text{-N}_2$ and $\alpha\text{-N}_2$ (~ 95 K and 145 K, respectively) found on $\text{Fe}(111)$ [10] that also points to the former as the weakly bound state.

V. SUMMARY

In summary, we have studied the dynamics of N_2 uptake by the $\text{Fe}(110)$ surface using a 6D *ab-initio* PES and classical trajectory calculations. Our results show that dissociative adsorption of N_2 at this surface is an activated process with a rather high minimum energy barrier of about 1.1 eV. The configuration associated to such minimum energy barrier is well defined and it corresponds to the molecule parallel to the surface, with the center of mass on the bridge site, and the axis of the molecule pointing towards the nearest hollow sites. Our 6D dynamics simulations confirm the transition state and activation energies reported in previous works that were based on reduced dimensionality calculations [15, 16]. Our results also support the conclusion of ref. 15 suggesting that the measured activation

energy of 0.28 eV [6] is probably due to dissociation occurring at steps and defects, and not on the pristine Fe(110) surface. Additionally, the results of our dynamics calculations show that the reaction path is very narrow. As a result, dissociative adsorption probabilities are lower than 2×10^{-5} for energies below 1.6 eV. These results explain the measured low reactivity of this system [5, 6]. It is worth to mention that this finding, showing that the Fe(110) inertness to N_2 dissociation is caused by the existence of large energy barriers close to the surface, has been also observed in other low reactive systems as N_2 /Ru(0001) [34], O_2 /Ag(100) [35] and, more recently, on O_2 /Ag(111) [36].

Interestingly, a rather complex dependence of the reactivity on the incidence conditions is observed, namely, the dissociation probability neither scales with the total incident energy of the molecule, nor with the normal incident energy. This behavior has been related to the existence of multiple energy barriers along the reaction paths: apart from the dominant activation barrier of about 1.1 eV, lower energy barriers of about 0.5-0.6 eV in the entrance channel are observed that impose a condition to the minimum normal energy required for the reaction to take place.

Using the generalized Langevin oscillator model, we have also incorporated energy dissipation and exchange with the lattice in the dynamics. This kind of calculations has allowed us to analyze the non-dissociative molecular adsorption process. We have identified two distinct molecular adsorption sites with adsorption energies that differ in about 100 meV: (i) one with the molecule located vertical to the surface on the top site at ~ 2.4 Å from the surface and (ii) the energetically most favorable adsorption site in which the molecule is parallel to the surface at a distance of ~ 1.4 Å over the hollow site. The static analysis of the energetics would suggest that the molecules would be adsorbed in the energetically most favorable state over hollow. However, our simulations demonstrate that this is not necessary the case and that only the dynamical study can provide an accurate knowledge of the final adsorption site. This is due to the presence of different energy barriers that the molecules have to overcome to be adsorbed in each of the two sites. In fact, we have shown that the final adsorption site depends on the molecular incident energy and on the surface temperature. More precisely, the top-vertical state with a minimum energy barrier of 150 meV is populated at low incident energies and surface temperatures. In contrast, when increasing the incidence energy and surface temperature, the molecules tend to populate the energetically most favorable adsorption state over hollow that has a larger energy barrier of

250 meV. The absence of molecular adsorption in thermal and hypothermal N_2 gas exposure experiments [13] is consistent with the energy barriers for N_2 uptake found in our dynamics simulations.

VI. ACKNOWLEDGEMENT

This work has been supported in part by the Basque Departamento de Educación, Universidades e Investigación, the University of the Basque Country UPV/EHU (Grant No. IT-366-07) and the Spanish Ministerio de Ciencia e Innovación (Grant No. FIS2010-19609-C02-02). Computational resources were provided by the DIPC computing center.

-
- [1] G. Ertl, Catal. Rev.-Sci. Eng **21**, 201 (1980).
- [2] M. Grunze, *The Chemical Physics of Solid Surfaces and Heterogenous Catalysis*, edited by D. King and D. Woodruff, Vol. 4 (Elsevier, New York, 1982) p. 142.
- [3] M. Alducin, R. Díez Muiño, H. F. Busnengo, and A. Salin, Phys. Rev. Lett. **97**, 056102 (2006).
- [4] G. A. Bocan, R. Díez Muiño, M. Alducin, H. F. Busnengo, and A. Salin, J. Chem. Phys. **128**, 154704 (2008).
- [5] F. Bozso, G. Ertl, and M. Weiss, J. Catal **50**, 519 (1977).
- [6] F. Bozso, G. Ertl, M. Grunze, and M. Weiss, J. Catal. **49**, 18 (1977).
- [7] M. Grunze, M. Golze, W. Hirschwald, H. J. Freund, H. Pulm, U. Seip, M. C. Tsai, G. Ertl, and J. Küppers, Phys. Rev. Lett. **53**, 850 (1984).
- [8] L. J. Whitman, C. E. Bartosch, W. Ho, G. Strasser, and M. Grunze, Phys. Rev. Lett. **56**, 1984 (1986).
- [9] M. C. Tsai, U. Ship, I. C. Bassignana, J. Küppers, and G. Ertl, Surf. Sci. **155**, 387 (1985).
- [10] M. Grunze, G. Strasser, and M. Golze, Appl. Phys A **44**, 19 (1987).
- [11] C. T. Rettner and H. Stein, Phys. Rev. Lett. **59**, 2768 (1987).
- [12] J. Bheim, W. Brenig, T. Engel, and U. Leutusser, Surf. Sci. **131**, 258 (1983).
- [13] K. Homann, H. Kuhlenbeck, and H. J. Freund, Surf. Sci. **327**, 216 (1995).
- [14] J. J. Mortensen, M. V. Ganduglia-Pirovano, L. B. Hansen, B. Hammer, P. Stoltze, and J. K. Nørskov, Surf. Sci. **422**, 8 (1999).
- [15] R. C. Egeberg, S. Dahl, A. Logadottir, J. H. Larsen, J. Nørskov, and I. Chorkendorff, Surf. Sci. **491**, 183 (2001).
- [16] A. Logadottir and J. K. Nørskov, Surf. Sci. **489**, 135 (2001).
- [17] S. Riikonen, A. S. Foster, A. V. Krashennnikov, and R. M. Nieminen, Phys. Rev. B **80**, 155429 (2009).
- [18] J. C. Tully, J. Chem. Phys. **73**, 1975 (1980).
- [19] H. F. Busnengo, A. Salin, and W. Dong, J. Chem. Phys. **112**, 7641 (2000).
- [20] G. Kresse and J. Furthmüller, Comput. Mater. Sci. **6**, 15 (1996).
- [21] G. Kresse and J. Hafner, Phys. Rev. B **47**, 558 (1993).

- [22] B. Hammer, L. B. Hansen, and J. K. Nørskov, Phys. Rev. B **59**, 7413 (1999).
- [23] G. Kresse and D. Joubert, Phys. Rev. B **59**, 1758 (1999).
- [24] M. Methfessel and A. T. Paxton, Phys. Rev. B **40**, 3616 (1989).
- [25] R. C. Weast, ed., *CRC handbook of chemistry and physics: a ready-reference book of chemical and physical data* (Boca Raton, Florida : CRC Press, 1986).
- [26] We check that the energy differs in only 20 meV when the N atom is located in the middle of the vacuum region.
- [27] M. Alducin, R. Díez Muiño, H. F. Busnengo, and A. Salin, J. Chem. Phys. **125**, 144705 (2006).
- [28] S. Pick, P. Légaré, and C. Demangeat, Phys. Rev. B **75**, 195446 (2007).
- [29] G. Volpilhac and A. Salin, Surf. Sci. **556**, 129 (2004).
- [30] A. Gross and M. Scheffler, Phys. Rev. B **57**, 2493 (1998).
- [31] H. F. Busnengo, M. A. Di Césare, W. Dong, and A. Salin, Phys. Rev. B **72**, 125411 (2005).
- [32] T. Ślęzak, J. Łażewski, S. Stankov, K. Parlinski, R. Reitering, M. Rennhofer, R. Rüffer, B. Sepiol, M. Ślęzak, N. Spiridis, M. Zajac, A. I. Chumakov, and J. Korecki, Phys. Rev. Lett. **99**, 066103 (2007).
- [33] J. P. Perdew, J. A. Chevary, S. H. Vosko, K. A. Jackson, M. R. Pederson, D. J. Singh, and C. Fiolhais, Phys. Rev. B **46**, 6671 (1992).
- [34] C. Díaz, J. K. Vincent, G. P. Krishnamohan, R. A. Olsen, K. Honkala, J. K. Nørskov, and G. J. Kroes, J. Chem. Phys. **125**, 114706 (2006).
- [35] M. Alducin, H. F. Busnengo, and R. D. Muiño, J. Chem. Phys. **129**, 224702 (2008).
- [36] I. Goikoetxea, J. Beltrán, J. Meyer, J. I. Juaristi, M. Alducin, and K. Reuter, New J. Phys. **14**, 013050 (2012).

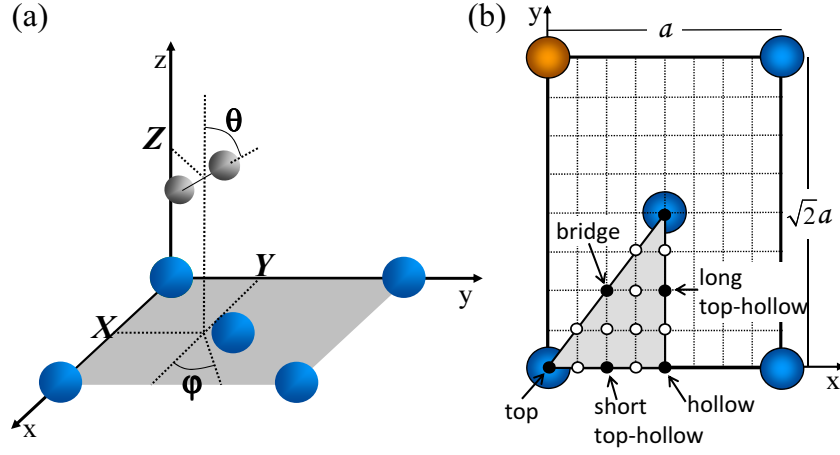


FIG. 1. (a) Coordinate system used in our calculations: Fe atoms are in red and the N_2 nuclei are in grey. (b) Geometry of the Fe(110) surface. DFT calculations of the $N/Fe(110)$ PES have been performed for all sites marked by white and black circles. For $N_2/Fe(110)$, DFT calculations have been performed for configurations with the molecular center over the sites marked by black circles. The shaded area shows the irreducible surface unit cell.

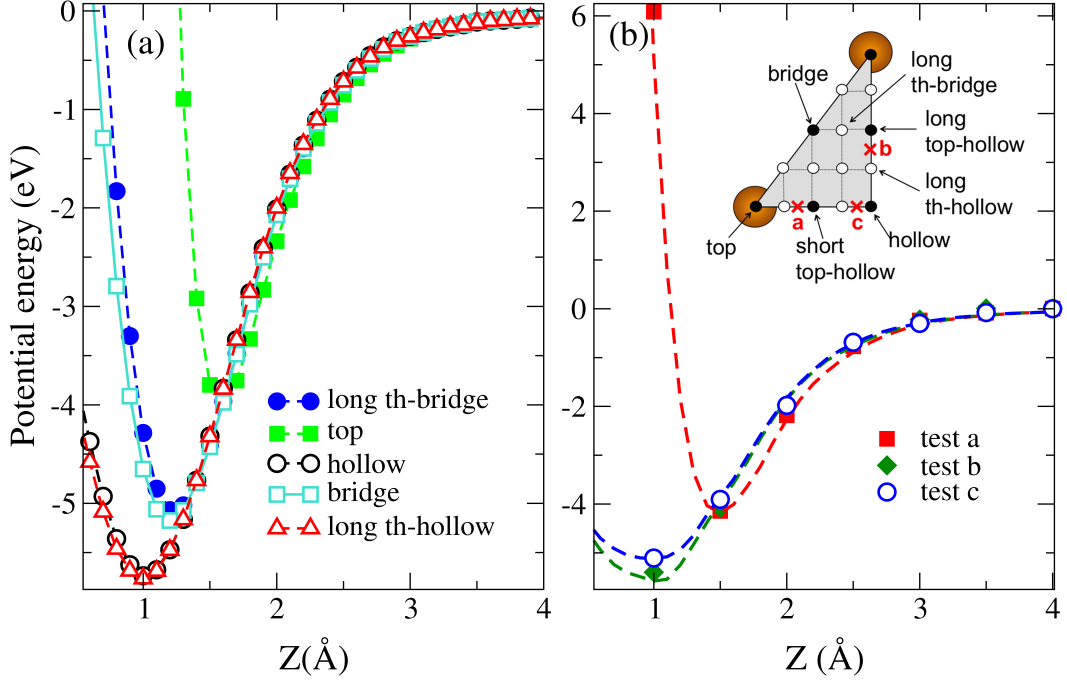


FIG. 2. (a) Dependence of the potential energy N/Fe(110) on the atom-surface distance Z_N , for different positions of the N atom over the surface unit cell. The DFT data are represented by symbols and the corresponding Z_N -interpolation by dashed lines. (b) Comparison between the DFT energies (symbols) and their corresponding interpolation values (dashed lines) for three configurations not used in the interpolation. The red crosses labeled as a, b and c in the irreducible unit cell identify the three sites used with testing purposes (test a, test b, and test c, respectively).

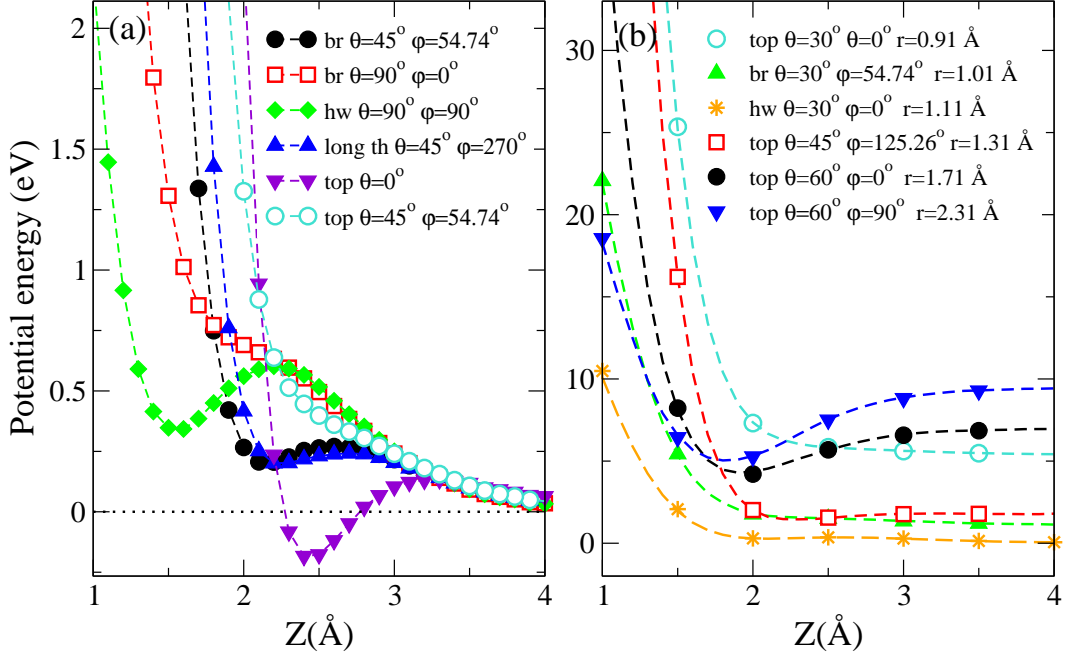


FIG. 3. (a) Dependence of the $\text{N}_2/\text{Fe}(110)$ potential energy on the distance of the molecular center from the surface Z for fixed X , Y , θ and φ . The internuclear distance is in all cases $r_{eq} = 1.11$ Å. The DFT energies are represented by symbols and the corresponding Z -interpolation by dashed lines. (b) Comparison between the DFT (symbols) and the interpolated (dashed lines) energies for various configurations not used as input data in the construction of the interpolated 6D PES. Notice that the internuclear distance is different in each case.

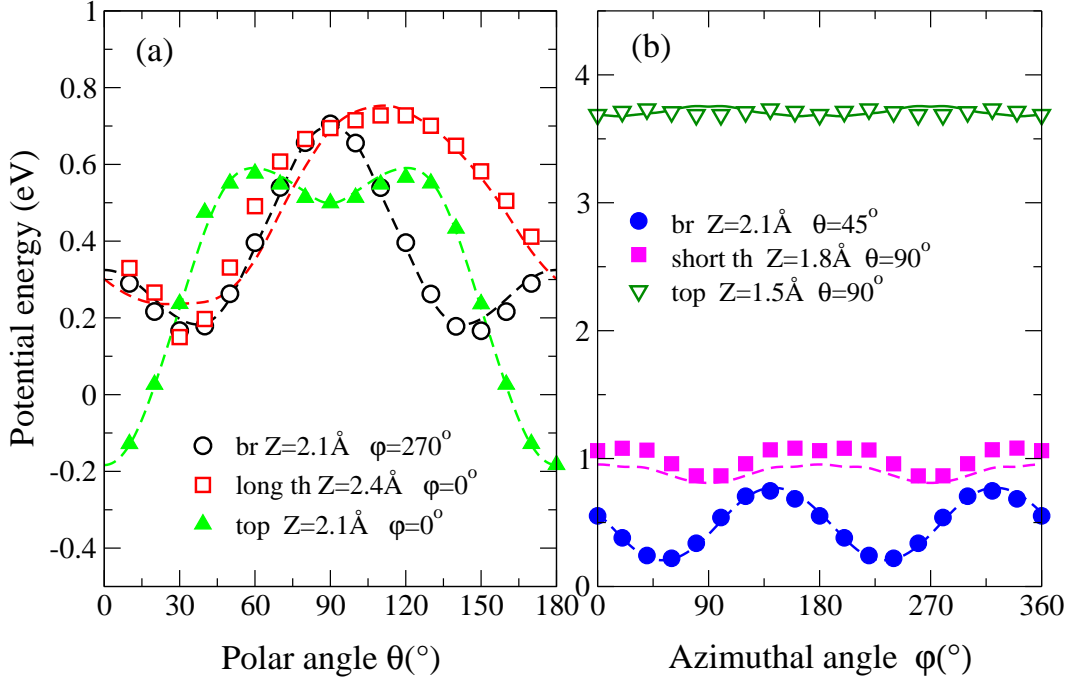


FIG. 4. Comparison between interpolated potential energies (dashed lines) and DFT values not used in the interpolation procedure (symbols). Variation with: (a) θ and (b) φ for various positions of the molecule. In all the cases, $r = r_{eq}$.

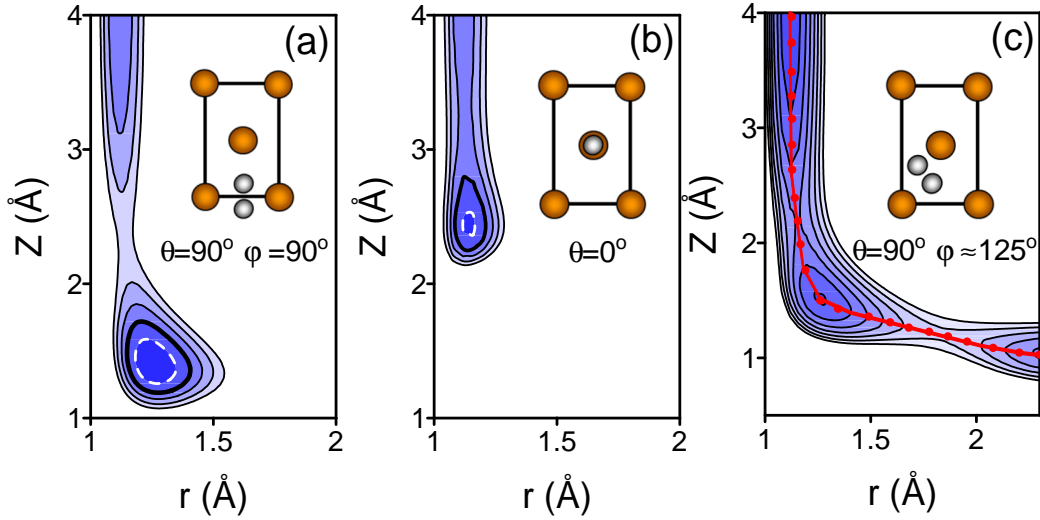


FIG. 5. Solid black (dashed white) lines correspond to positive (negative) values of potential energy. Thick solid lines correspond to zero potential energies. The molecular orientation and position over the surface unit cell is schematically depicted in each contour plot. Contour lines separate intervals of 0.2 eV. The 2D dissociation path is marked in red in (c).

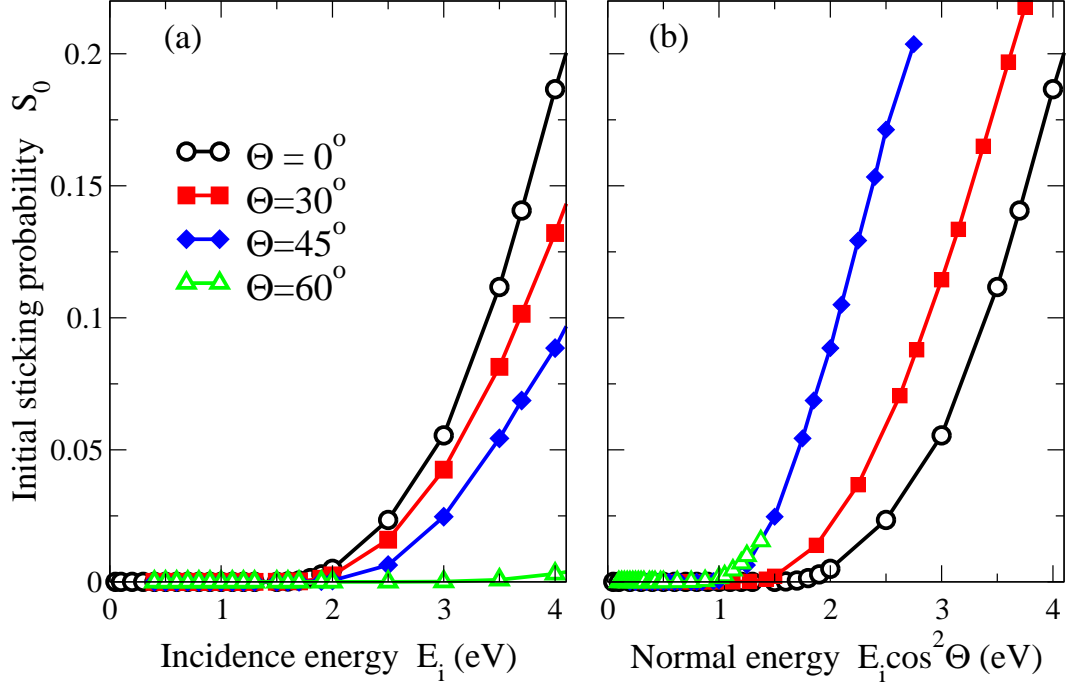


FIG. 6. (a) Initial dissociative sticking probability S_0 as a function of the initial kinetic energy E_i for different incident angles Θ . (b) S_0 as a function of the normal incident kinetic energy.

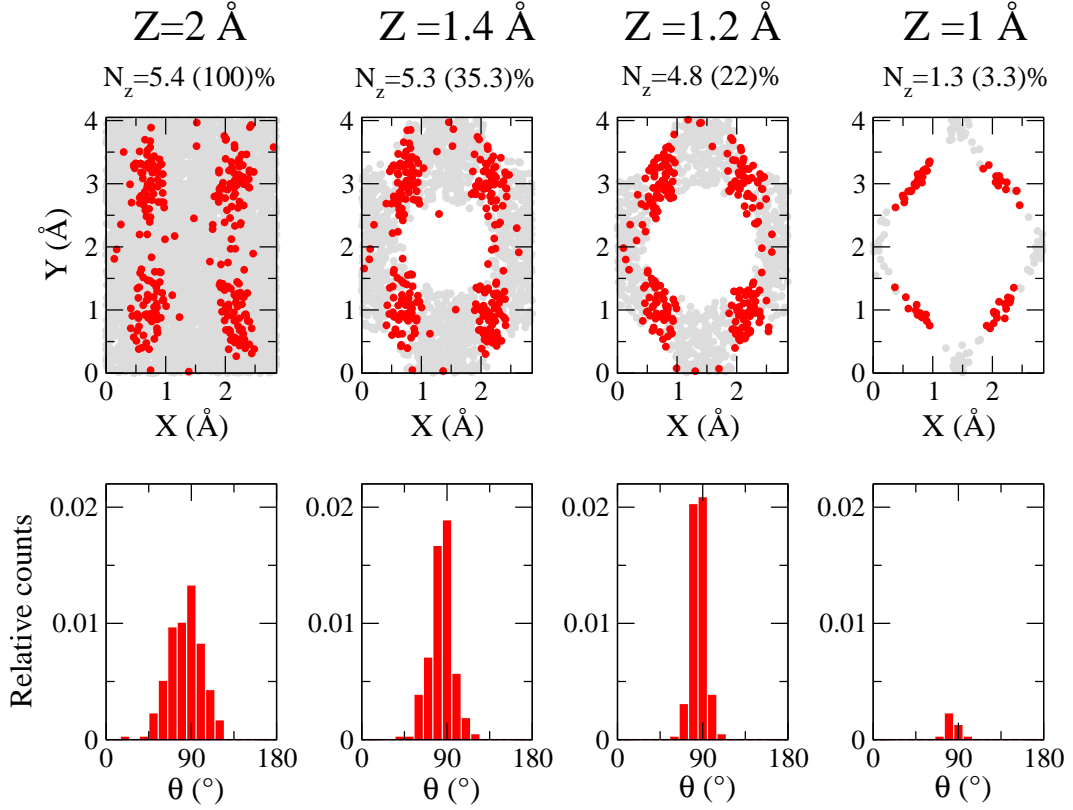


FIG. 7. Evolution of N_2 on the Fe(110) surface for 5000 trajectories. The incidence conditions are $E_i = 3 \text{ eV}$ and $\Theta = 0^\circ$. Top panel: position of the molecule center of mass over the surface unit cell when first reaching a distance Z from the surface. The dissociating and reflecting molecules are plotted in red and grey circles, respectively. On top of each panel, N_z is the fraction of dissociated molecules reaching Z , while the total percentage of molecules at each Z is written within the parenthesis. Low panel: associated normalized θ -distribution of the dissociating molecules.

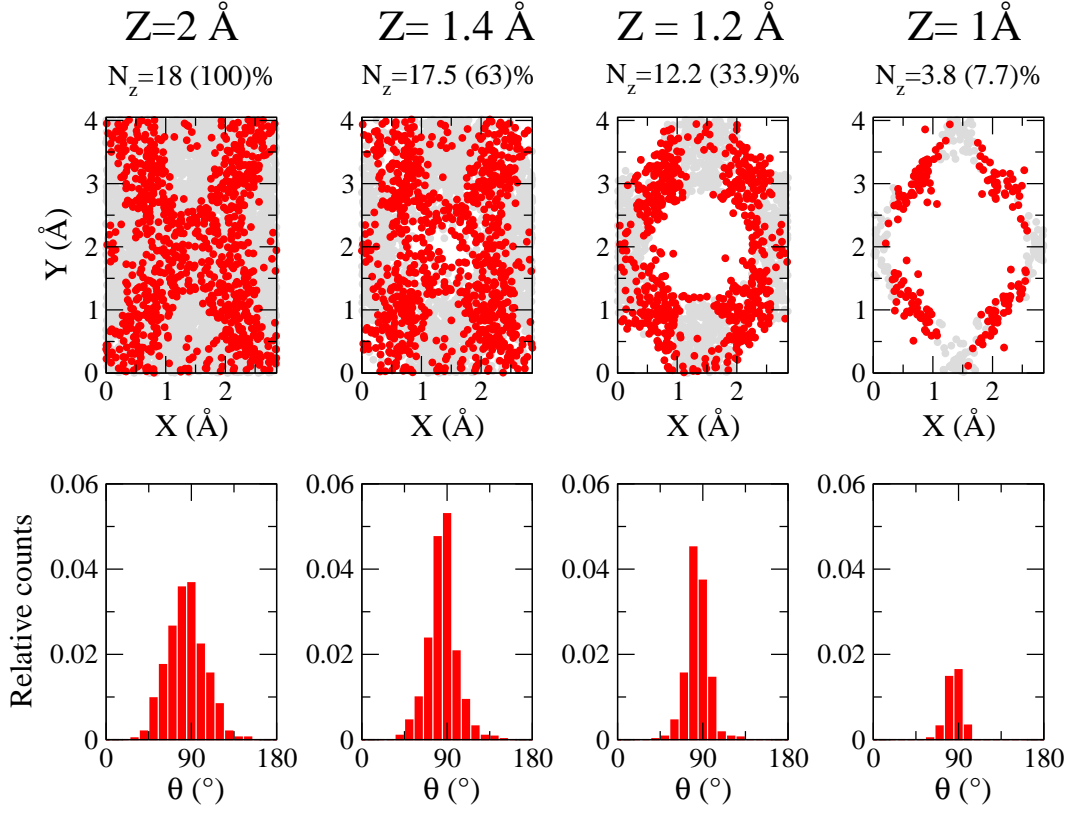


FIG. 8. Same as Fig. 7 for incidence conditions $E_i=4$ eV and $\Theta = 0^\circ$

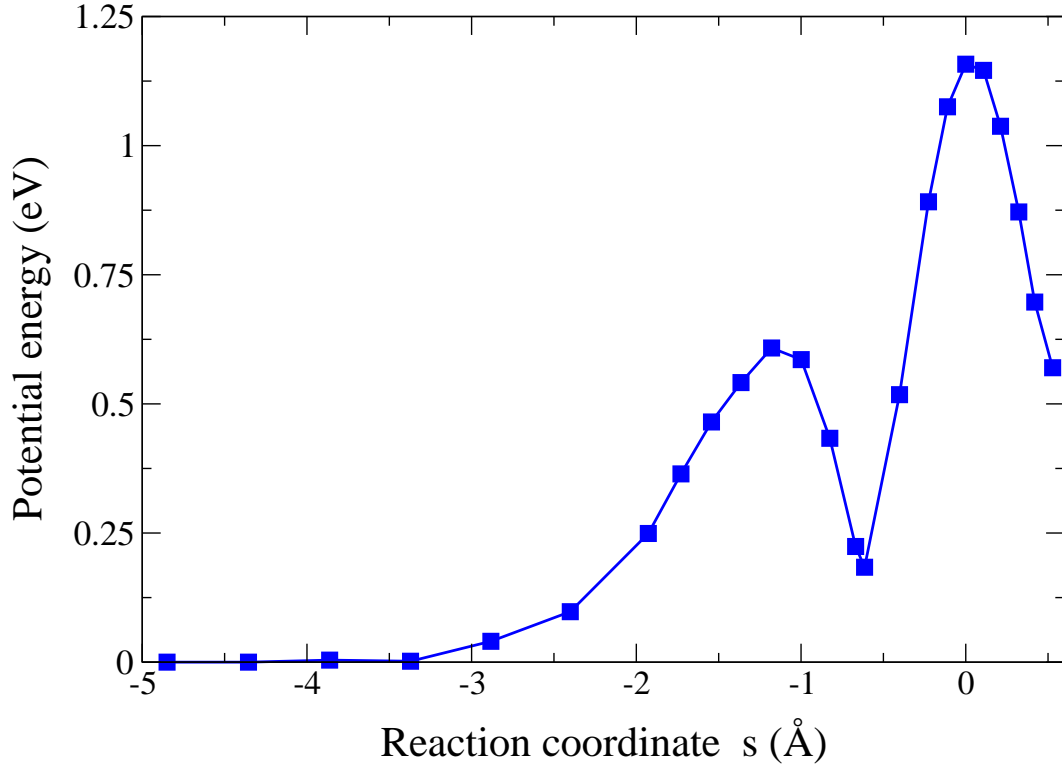


FIG. 9. Potential energy as a function of the reaction coordinate s , defined as the distance in the (Z,r) space from the position of the minimum energy barrier to dissociation ($s=0$) along the minimum energy path in 2D. Negative (positive) values correspond to points reached by the incoming molecule before (after) the transition state. The points used to obtain the potential energy curve are marked with full circles in Fig. 5(c).

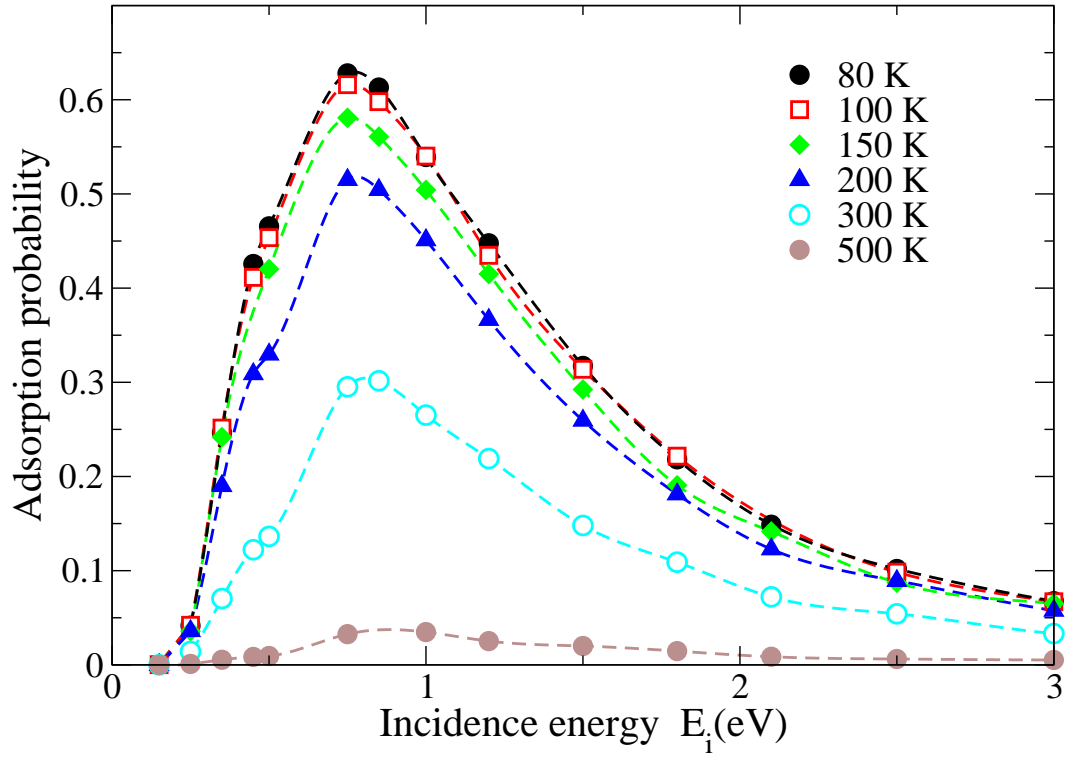


FIG. 10. Molecular adsorption probability (see text) as a function of the incident energy, for different surface temperatures and normal incidence.

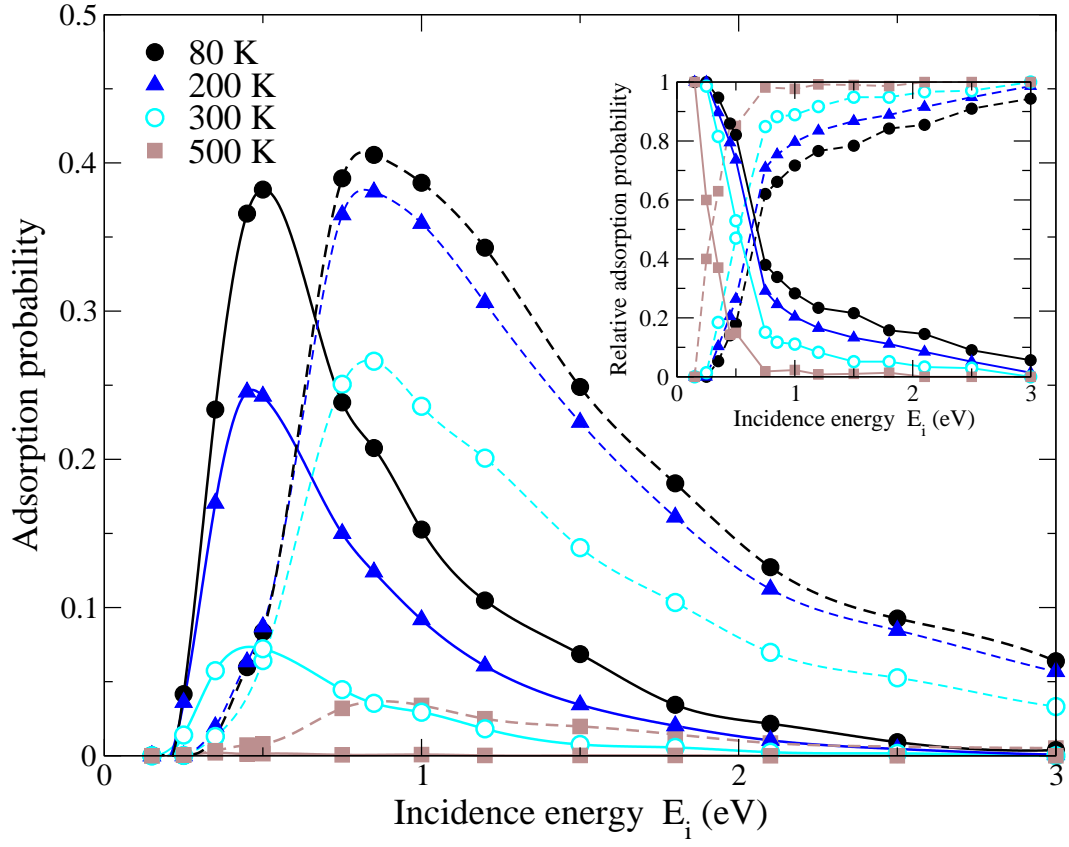


FIG. 11. Molecular adsorption probability in each of the two adsorption wells as a function of the incident energy for different surface temperatures and normal incidence. Solid (dashed) lines represent the adsorption probability on the top (hollow) well. The fraction of molecules adsorbed in each well is shown in the inset.